Polar Ionospheric Imaging at Storm Time

Ms Ping Yin and Dr Cathryn Mitchell
Department of Electronic and Electrical Engineering
University of Bath
BA2 7AY
UNITED KINGDOM

p.yin@bath.ac.uk / eescnm@bath.ac.uk

Dr Gary Bust
ARL University of Texas
USA

gbust@arlut.utexas.edu

ABSTRACT

During periods of major geomagnetic storms the polar ionosphere becomes very variable. Ground-based measurements, such as NIMS, GPS or ionosonde data are too sparse to do tomographic imaging, however, combination of these data sources as well as other available measurements, such as satellite-based data, may have the possibility to monitor the structure of the disturbed polar ionosphere. In this paper, LEO-based GPS data onboard CHAMP as well as ground-based GPS and ionosonde observations are input into a four dimensional tomographic algorithm – MIDAS (Multi-Instrument Data Analysis System) to image the disturbed ionosphere at Alaska and Greenland as well as over Europe for the major storm in October 2003. In contrast, electron density images produced by another independent method – IDA3D (Ionospheric Data Assimilation Three Dimensional), which assimilates primarily NIMS data and other data source, are involved to perform comparisons. A general good agreement can be obtained between them. As a result, the addition of LEO-based GPS data presents a great potential in polar ionospheric imaging.

1.0   INTRODUCTION

Tomographic imaging is an established method to study the ionosphere [for example see 1, 2]. Because the GPS coverage at the higher latitudes is relatively sparse due to the orbital inclination of the GPS constellation, it is difficult to image the ionosphere there with tomographic techniques using only ground-based GPS data. With the development of the radio-occultation technique in ionospheric imaging [3], however, the characteristics of the polar ionosphere at the storm-time are expected to be represented better with occultation data. Radio-occultation measurements observed by Low earth orbiters (LEO) have been adopted to improve ionospheric tomography [4]. In this study, we use both navigation and occultation measurements onboard the LEO CHAMP to make the inversion.

Using the CHAMP navigation and occultation data and some available ionosonde data, in conjunction with a 4D tomographic method (MIDAS) [5], images of electron density over Greenland and Alaska and the high latitudes over Europe are generated for periods of the October 2003 storm. A comparison between different data sources for imaging, such as GPS/CHAMP/ionosonde measurements, is made. Experimental results of using radio occultation data for imaging the disturbed ionosphere have been discussed previously by Yin et al [6].

For verification purposes, images in the same region are produced by another tomographic algorithm - Ionospheric Data Assimilation Three Dimensional (IDA3D) [7] with NIMS data, ground-based and space-based GPS measurements. NIMS data are excellent for producing 2-D images of the ionosphere but are limited by the number of suitable satellite passes. By comparing between images reconstructed with GPS, GOS and GIOS (see their representation in the 4.0 section) results, the advantages of using occultation/navigation data over the polar region are clearly identified.

2.0 METHOD

Since the ionosphere is dispersive in nature, either the code or the phase delay in the GPS signals is proportional to the inverse of the squared frequency and directly proportional to the change in TEC. For dual-frequency GPS receivers, the differential phase shift is formed from linear combinations of carrier phases at L1 and L2, as shown in the following equation,

$$\phi_{L1} - \phi_{L2} = 40.3 \times (\frac{1}{f_{L2}^{2}} - \frac{1}{f_{L1}^{2}}) \times TEC + \varepsilon_{\phi}$$

in which Φ_{L1} and Φ_{L2} are the phase delays of L1 and L2 respectively, f_{L1} and f_{L2} are GPS two carrier frequencies, TEC is the relative slant TEC values and ε_{Φ} is the residual errors including integer ambiguities in addition to multi-path and inter-frequency biases. Therefore, calibration is needed if accurate GPS TEC will be used to image the ionosphere due to the residual errors. In this study, ground-based and space-based GPS data are firstly bias-corrected to remove most of biases including the satellite-receiver inter-frequency biases. Then calibrated GPS data are re-input into MIDAS to image the disturbed ionosphere for the 29 and 30 October 2003 storm.

As is well described in [5], the MIDAS inversion algorithm which is used in this study requires a priori assumptions to image the ionosphere. For the storm conditions, an extended range of Chapman profiles with a range of scale heights and peak heights is set to construct the background ionosphere during storms. Then as in the standard method, spherical harmonics are applied concerning the horizontal variations, and EOFs (Empirical Orthonormal Functions) are generated to represent the vertical distribution of ionization.

Finally, the reconstructed inversion results, for example, the electron concentration distribution and total electron content (TEC) variation against latitudes/longitudes will be shown hourly in forms of maps with 1° (Latitude)× 4° (Longitude) × 50 km (Altitude) grid voxels extending from 80 to 1080 km above the earth.

3.0 MEASURMENTS

The observational inputs to MIDAS include ground-based GPS measurements (phase and time delay) that are available from SOPAC (Scripps Orbit and Permanent Array Center). In this study, ground GPS receivers are selected from 160ºW to 40ºE in longitude and 50ºN to 80ºN in latitude. Space-based GPS measurements and occultation data onboard LEO/CHAMP are supplied by the ISDC (Information System and Data Center, GFZ) and the ground ionosondes data are available from the SPIDR (Space Physics Interactive Data Resource). Table 1 lists the available ionosondes for this storm.

Table 1: Ionosondes locations

Ionosonde code	Station name	Geographic Latitude	Geographic Longitude
THJ77	Thule/Qaanaaq	77.5ºN	69.2ºW
KS759	King Salmon	58.4ºN	156.4ºW
NQJ61	Narssarssuaq	61.2ºN	45.4ºW
JR055	Juliusruh/Rugen	54.6ºN	13.4ºE
TR169	Tromso	69.7ºN	19.0ºE
FF051	Fairford	51.7ºN	1.5ºW

The data used are:

Ground-based GPS receivers observations with 30 seconds data interval; Space-based GPS receiver onboard CHAMP satellite, that is, GPS code and carriers phase data records including occultation data with 1Hz sample rate and GPS RINEX data with 10 sec sample rate. These data were processed for the period of 28 to 31 October 2003, here we focus on the 29th and 30th that are the main phases of this storm.

4.0   RESULTS AND DISCUSSIONS

The results description as shown in Table 2 explains the notation used for the different data combinations. GPS is used to represent the inversion images from ground-based GPS data alone, GOS represents the reconstructed images from the combination of ground-based GPS and CHAMP occultation and navigation data, while GIOS stands for the inversion results from ground-based GPS, CHAMP (occultation and navigation) and ionosonde data.

Table 2: Inversion results representation in terms of their input data

Results	Ground-based GPS	CHAMP observations	Ionosondes
GPS	×		
GOS	×	×	
GIOS	×	×	×

4.1   29 October 2003 Storm

For the storm on 29th October, the focus is put on the analysis of the addition of CHAMP data, which is investigated from the two aspects, that is, with a CHAMP pass and without a CHAMP pass in that area. The areas of interest are concentrated on the higher latitudes, in particular, Greenland and Alaska.

Hourly TEC maps reconstructed by CHAMP navigation/occultation data over the northern hemisphere on 29 October 2003 is shown in Figure 1, from which the CHAMP traces can be identified. For example, The CHAMP passed over Alaska and Greenland at 0900, 1100, 2000, 2200 UT and 0300, 0500, 1400, 1600 UT, respectively.
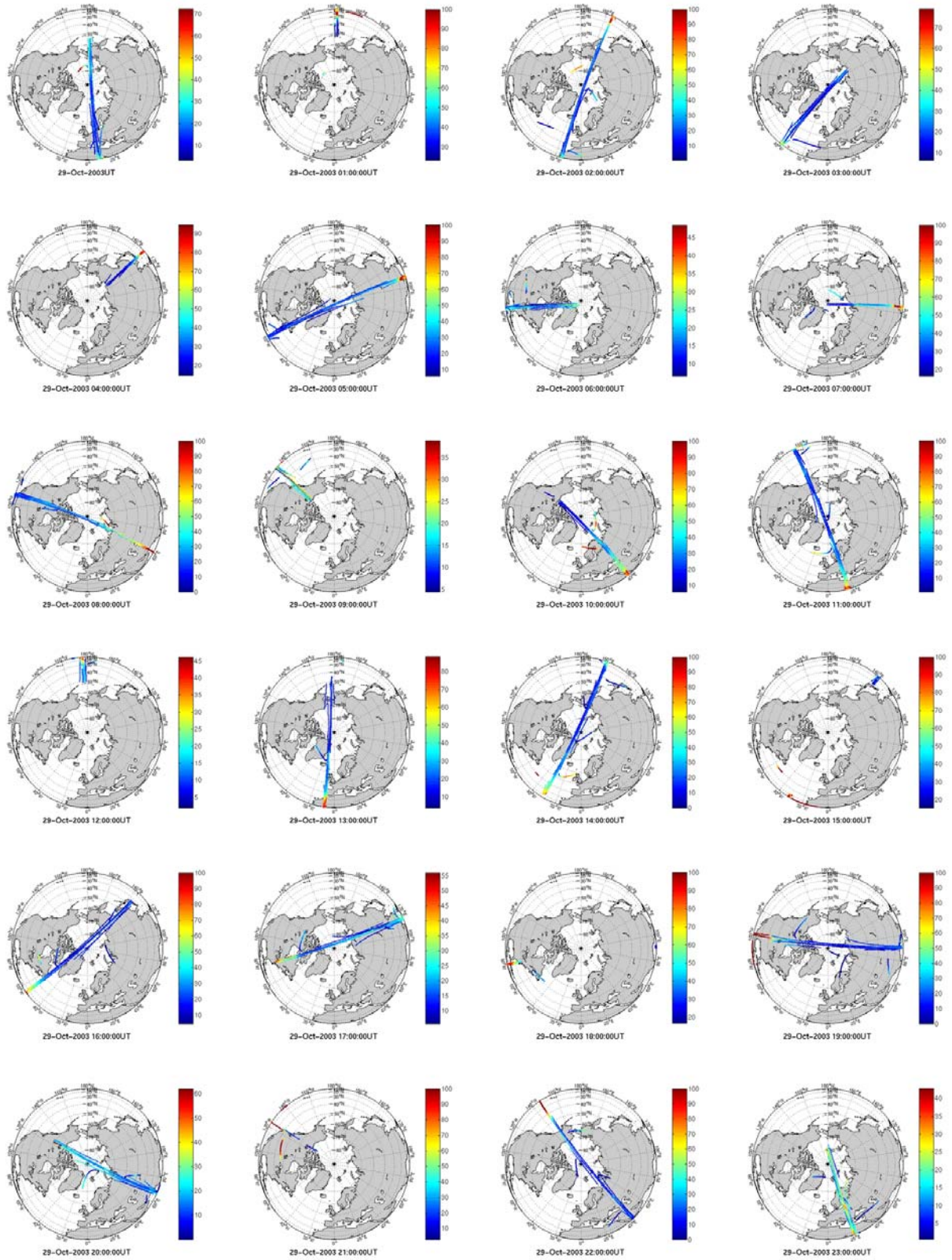
Figure 1: Hourly CHAMP TEC maps over the northern hemisphere on 29 October 2003

4.1.1 Without CHAMP Passes

The effect of additional CHAMP data is considered when there was no CHAMP pass over that region. As can be seen from CHAMP passes over the north hemisphere on 29 October in Figure 1, the images over Alaska at 0700 UT and those over Greenland at 2200 UT are selected to present the results when there is no CHAMP passes. The latitude range of the images is from 50ºN to 80ºN over Alaska, while 60ºN to 90ºN were selected for Greenland.
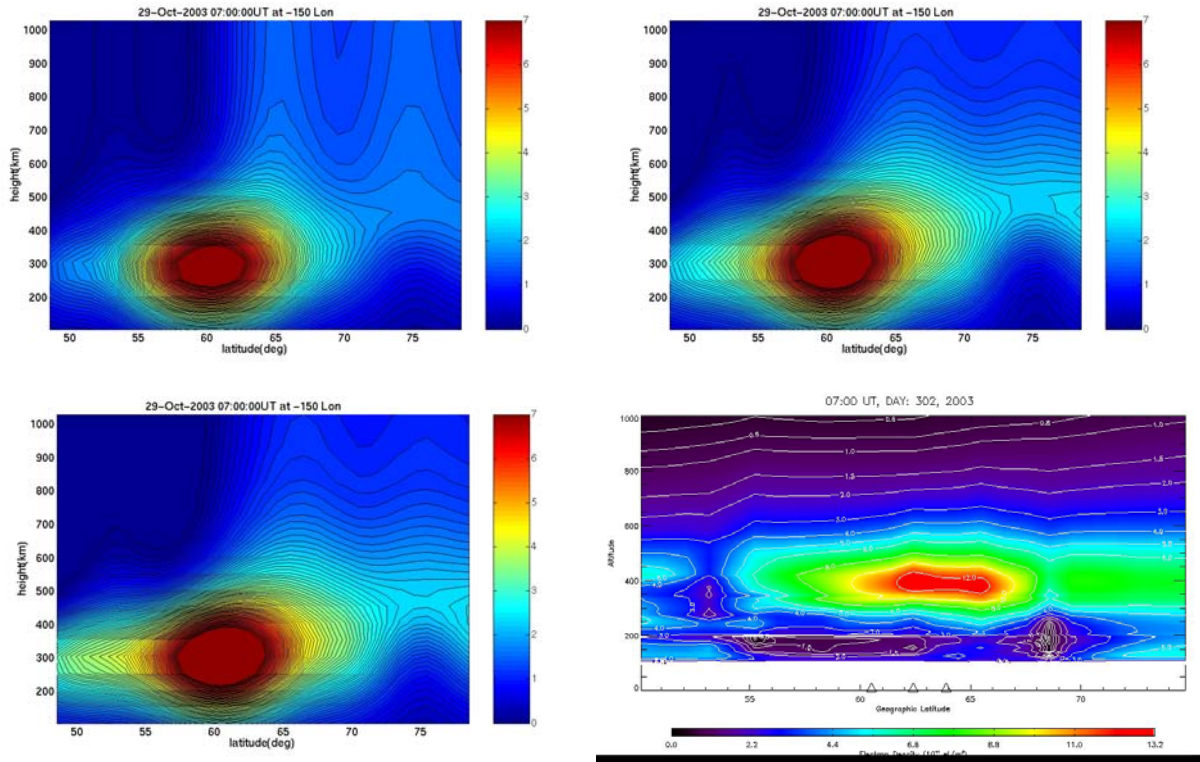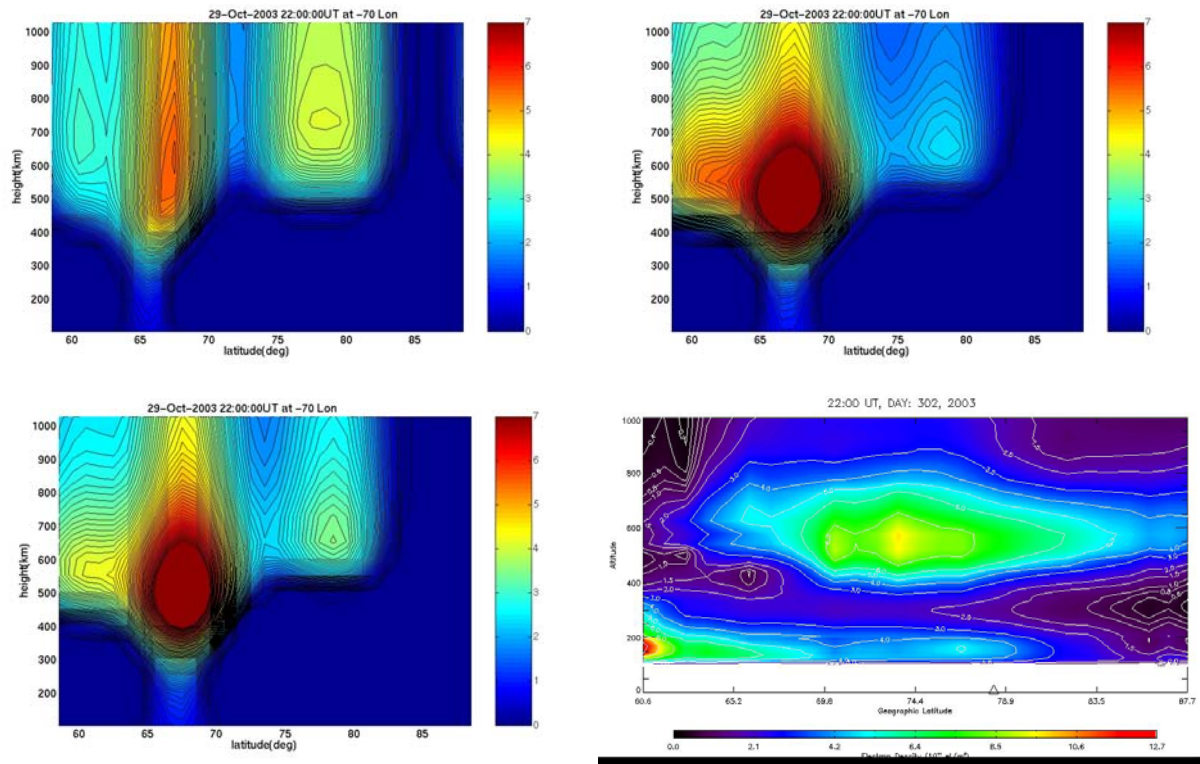

Figure 2: Electron density images over Alaska at 0700 UT on 29 October (top left: GPS results; top right: GOS results; bottom left: GIOS results; bottom right: NIMS results)

When there is no CHAMP pass over the region, the addition of occultation and navigation data has little effect on the final images in terms of the vertical profile, but the electron density shows some difference, indicating that the data input from another region can have an effect over the entire image. The images over Alaska at 0700 UT as shown in Figure 2 which derived from calibrated GPS, GOS and GIOS results respectively, are nearly the same at all latitudes. They all see the electron density enhancement around 60ºN, which is also observed in the NIMS image as shown in the bottom right panel in Figure 2, in which triangles on the X-axis stand for the location of NIMS receivers.

Furthermore, all of the images over Greenland at 2200 UT from GPS, GOS and GIOS results in Figure 3 present the ionospheric uplift to 700 km at 78ºN. However, it is apparently not effected by the contribution of CHAMP occultation and navigation data since there is no difference in the region above 75ºN among the GPS/GOS/GIOS reconstructed images. This is interesting because it indicates that the ground-based GPS data contains information about the vertical profile of the electron density. This may be more the case at high latitudes where the rays are predominantly at low elevations.
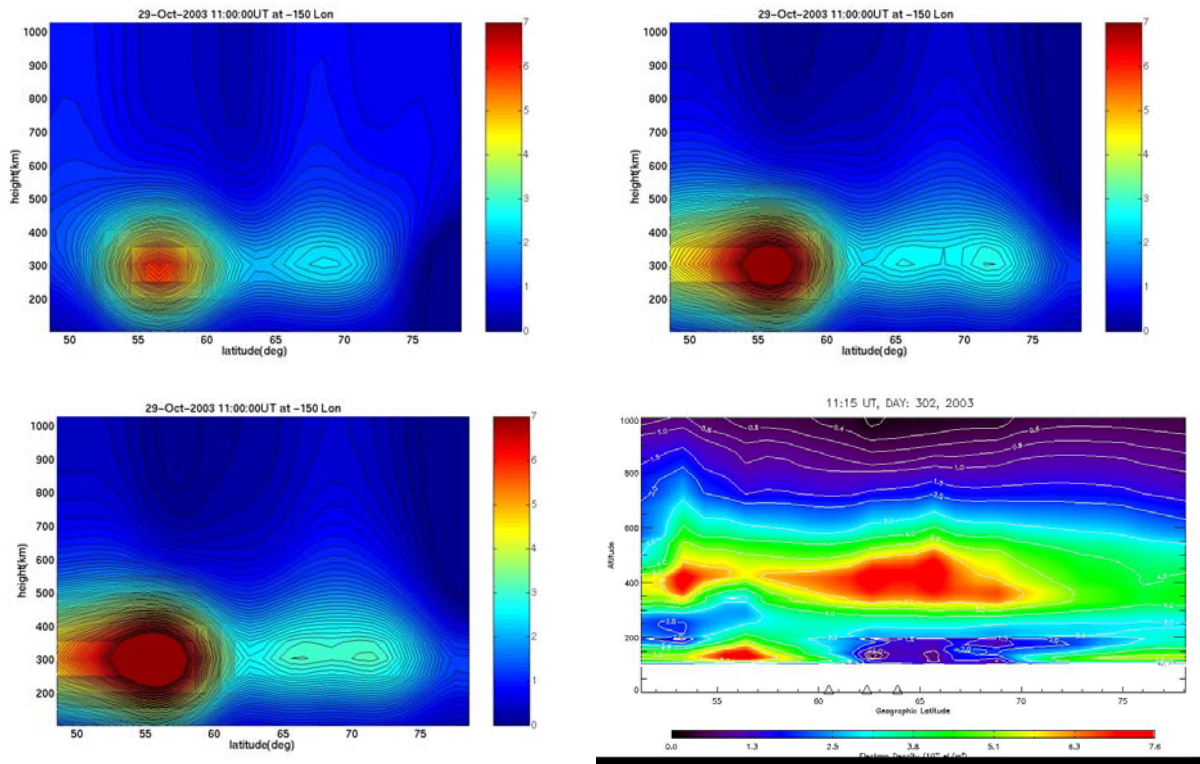
Figure 3: Electron density images over Greenland at 2200 UT on 29 October (top left: GPS results; top right: GOS results; bottom left: GIOS results; bottom right: NIMS results)

4.1.2 With CHAMP Passes

As can be seen from CHAMP passes over the north hemisphere on 29 October in Figure 1, the images over Greenland at 1400 UT and those over Alaska at 1100 UT are selected to present the advantage of CHAMP measurements.
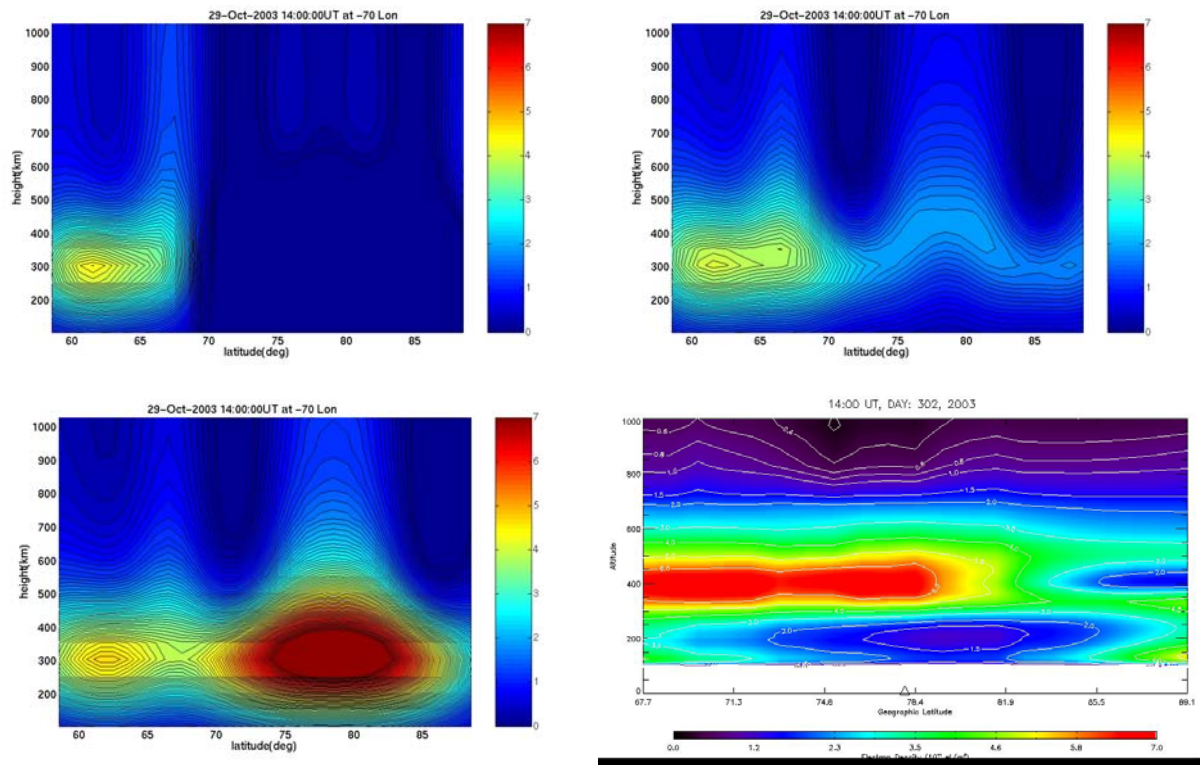
Figure 4 illustrates electron density distribution produced from calibrated GPS, GOS and GIOS inverted results, respectively. Electron concentration is plotted as a function of geographic latitudes and altitude at 1100 UT on 29 October over Alaska. The bottom right panel in Figure 4 shows the electron density image at 1115 UT over Alaska produced by mainly NIMS inverted results, which is used for verification purpose.

Figure 4: Electron density images over Alaska at 1100 UT on 29 October (top left: GPS results; top right: GOS results; bottom left: GIOS results; bottom right: NIMS results)

From comparisons among the above images, we can see that starting at 53ºN there is an electron density peak clearly seen from the NIMS image in Figure 4, which is also shown in GOS and GIOS images (see Figure 4). However this peak moves to higher latitude (above 55ºN) in the reconstructed GPS image (see the top left panel). Besides, further north there is another electron density peak around 65ºN, which is clearly seen in the NIMS image. Again from the top right and bottom left panels, we can observe this peak at exactly 65ºN, but in the GPS reconstructed image, this peak moved to 68ºN. Hence, a conclusion can be made that the GOS/GIOS reconstructed images represent the ionospheric distribution more accurately than GPS reconstructed images.

Figure 5: Electron density images over Greenland at 1400 UT on 29 October (top left: GPS results; top right: GOS results; bottom left: GIOS results; bottom right: NIMS results)

Furthermore, GOS/GIOS results are much better in regions above 70ºN where GPS ground measurements are in lack, which we can tell from the following images over Greenland. Figure 5 illustrates electron density distribution produced from calibrated GPS, GOS and GIOS inverted results, respectively. They are plotted at 1400 UT on 29 October over Greenland. In addition, as a reference, the bottom right panel in Figure 5 also shows the image of electron density from NIMS results at the same time over Greenland.

As compared to the NIMS image, the GPS reconstructed image shown in the top left panel does not exactly reproduce the distribution of electron density above 70ºN latitudes. This can be proved by the occurrence of electron density peak around 78ºN in the NIMS image, which is not seen in the GPS reconstructed image. However, those GOS/GIOS images (the top right and bottom left panels) produced with the assimilation of CHAMP occultation/navigation data into ground GPS data greatly improved the ionospheric images of electron density in the higher latitudes where CHAMP passed. They both show the density peak except for a bit different peak height. The peak height derived from the GOS results (about 400 km) is similar to that from the NIMS results. The addition of ionosonde measurements may make the electron density greater, particularly the peak density.

4.2   30 October 2003 Storm

For the storm on the 30th, the area of interest is focused on the electron density images at Svalbard in the late evening, where the simultaneous EISCAT scan can be obtained from the Madrigal database.
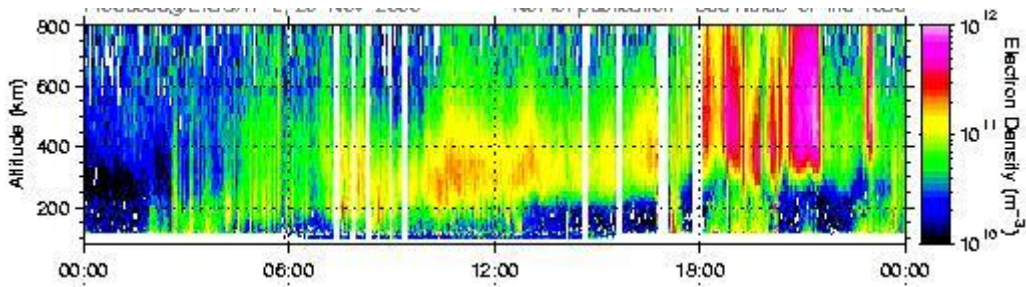
Figure 6: EISCAT scan at Svalbard on 30 October 2003

The electron density image as a function of altitude and time (UT) obtained with the EISCAT radar at Svalbard (78ºN and 16ºE) is shown in Figure 6. It can be clearly seen that electron densities are increased after 1800 UT on 30 October. In particular, the F layer height elevated above 500 km with the enhancement in electron densities around 2100 UT. In contrast, Figure 7 shows calibrated GIOS reconstructed images at 1900 - 2200 UT on 30 October. Here the images were generated by calibrated GIOS results in that the ESR is located at the high latitude where the ionosphere is represented well by calibrated GIOS results. The image at 2100 UT coincides with the ESR scan very well, where they both present the uplifts of the F-layer in conjunction with the electron density increase. The uplift in the peak height was also observed over the USA for the July 2000 storm [8].
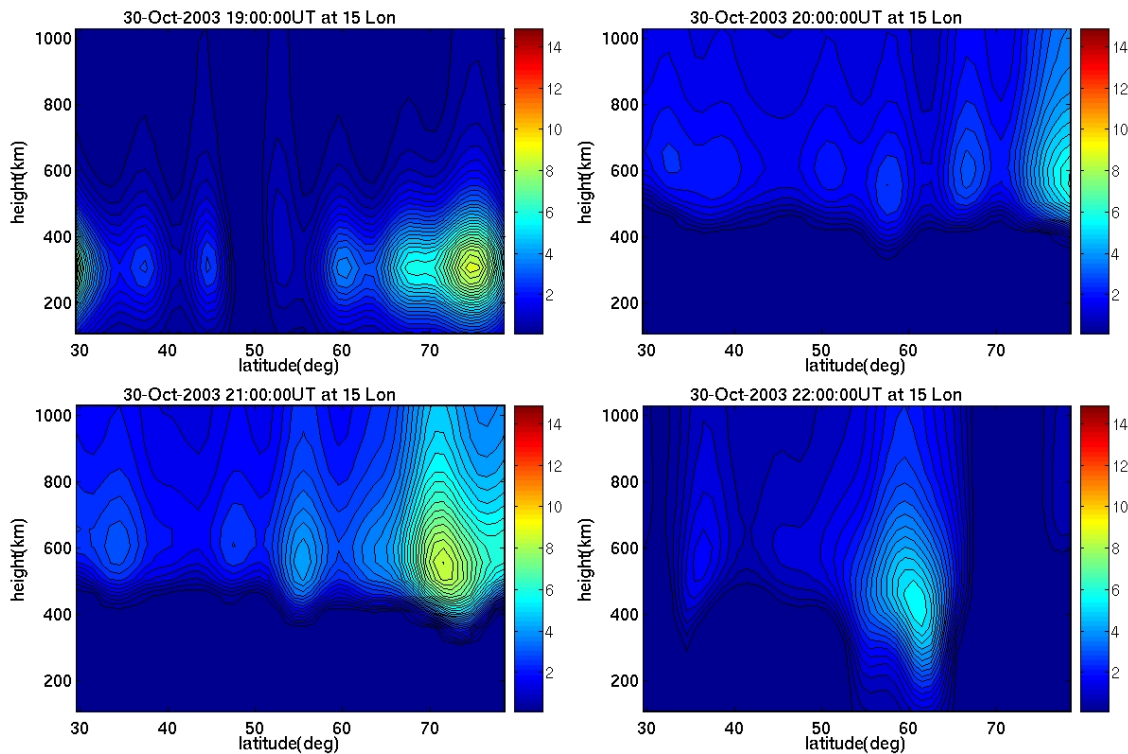

Figure 7: Images reconstructed from GIOS results at 15°E for 1900 - 2200 UT on 30 October

5.0   SUMMARY

The 29 October 2003 storm was chosen to compare GPS/GOS/GIOS reconstructed images by means of the verification of NIMS images over the polar region. The results indicate that GOS/GIOS reconstructed

images show good agreement with the NIMS images when CHAMP passed that area. The addition of CHAMP occultation data can improve the imaging of the detailed structure in the disturbed ionosphere over the polar region because of the shortage of the ground-based GPS receivers there.

Ionosondes are also sparsely distributed at the high latitude regions. There is only one available over Greenland (NQJ61 with 61.2ºN and 45.4ºW) on 29 October, while another one over Alaska (KS759 with 58.4ºN and 156.4ºW) was unavailable for the selected times on 29 October. This accounts for the similar images between GOS/GIOS results over Alaska, however, those images over Greenland have a difference in electron density. Thus, ionosonde data has some effect on the distribution of the electron density, in particular, increasing the peak density.

In summary, the images derived from GOS/GIOS results resemble the NIMS images much better than those from GPS results, which are lower resolution and less accurate at higher latitudes due to the shortage of ground receivers. In terms of the peak height, there seems no big difference among GPS, GOS and GIOS results. This may be due to the predomination of low-elevation rays from ground-based GPS there. The addition of CHAMP data into the tomographic algorithm greatly improved the details in ionospheric images over the polar region, e.g., from GOS images over Greenland, the electron density enhancement can be seen over the auroral and polar regions (above 65ºN), but there is little information from GPS reconstructed images due to the lack of GPS receivers there.

Dramatic uplifts in the F-layer at the high latitudes over Europe for the periods of 2000 – 2100 UT are captured by the reconstructed images, which are validated by the correspondent ESR scan. Meanwhile, the abnormal enhancement in electron-density in the local evening was also observed by the inverted images and the ESR scan, which may be attributed to the plasma convection from the mainland USA [9].

6.0   ACKNOWLEDGEMENT

7.0   REFERENCES

[1]   Fremouw E. J., Secan J. A. and Howe B. M. (1992). *Application of Stochastic inverse theory to ionospheric tomography.* Radio Science, 27 (5), 721-732.

[2]   Bernhardt, P. A., et al. (1998). *Two dimensional mapping of the plasma density in the upper atmosphere with computerized ionospheric tomography (CIT).* Physics of Plasmas, 5, 2010-2021.

[3]   Hajj G. A., Ibańez-Meier R., Kursinski E. R. and Romans L. J. (1994). *Imaging the ionosphere with the Global Positioning System.* Int. J. Imag. Syst. Technol. 5, 174.

[4]   Rius A., Ruffini G. and Cucurull L. (1997). *Improving the vertical resolution of ionospheric tomography with GPS occultations.* Geophys. Res. Lett. 24 (18), 2291-2294.

[5]   Mitchell, C. N. and Spencer P. S. (2003). *A three dimensional time-dependent algorithm for ionospheric imaging using GPS. Ann.* Geophysice-ITALY, 46 (4), 687.

[6]   Yin, P. and Mitchell C. N. (2005). *Use of radio-occultation data for ionospheric imaging during the April 2002 disturbances.* GPS Solutions, 9 (2), 156-163.

[7]   Bust G. S., Garner T. W., Gaussiran II T. L. (2004). *Ionospheric Data Assimilation Three-Dimensional (IDA3D): A global, multisensor, electron density specification algorithm.* J. Geophys. Res., 109, A11312, doi: 10.1029/2003JA010234.

[8]   Yin, P., Mitchell C. N., Spencer P. S. and Foster J. C. (2004*). Ionosperic electron concentration imaging using GPS over the USA during the storm of July 2000.* Geophys. Res. Lett., 31, L12806, doi: 10.1029/2004GL19899.

[9]   Mitchell C. N., Alfonsi L., De Franceschi G., et al. (2005). *GPS TEC and scintillation measurements from the polar ionosphere during the October 2003 storm.* Geophys. Res. Lett., 32 (12), Art. No. L12S03.